ISSN 1990-7931, Russian Journal of Physical Chemistry B, 2023, Vol. 17, No. 1, pp. 113–121. © Pleiades Publishing, Ltd., 2023.
Russian Text © The Author(s), 2023, published in Khimicheskaya Fizika, 2023, Vol. 42, No. 2, pp. 143–153.

ELECTRIC AND MAGNETIC PROPERTIES OF MATERIALS

Computer Simulation of a Silicene Anode on a Silicone Carbide Substrate

A. E. Galashev[a, b, *]

[a] *Institute of High Temperature Electrochemistry, Ural Branch, Russian Academy of Sciences, Yekaterinburg, Russia*
[b] *Yeltsin Ural Federal University, Yekaterinburg, Russia*
**e-mail: galashev@ihte.uran.ru*

Received April 12, 2022; revised July 4, 2022; accepted July 20, 2022

Abstract—The structures of two-layer silicene and the 4H-modified silicon carbide (SiC) film supporting it, which act as the anode of a lithium-ion battery, are studied by the molecular dynamics method. The behavior of such a combined anode is considered under conditions of its vertical filling with lithium. The silicene sheets contain vacancy defects in the form of bi-, tri-, and hexavacancies. Lithium ions directed perpendicularly to the silicene plane deposited on the silicene sheets remain in the silicene channel and partially penetrate the substrate surface. The vertical displacements of atoms in the top sheet of silicene after lithium intercalation significantly exceed the corresponding displacements in the bottom sheet in contact with the substrate. The construction of Voronoi polyhedra (VP) separately for the Si- and C-subsystems of SiC make it possible to reveal the structural features of each of the subsystems of the studied two-dimensional layered structure.

Keywords: anode, silicon carbide, Voronoi polyhedron, molecular dynamics, silicene, structure
DOI: 10.1134/S1990793123010190

INTRODUCTION

Theoretically, the use of silicon instead of carbon as the anode material of a lithium-ion battery (LIA) can increase the capacity of this electrode by an order of magnitude [1]. However, the volume of the silicon electrode increases significantly (by a factor of 3) after lithium intercalation [2]. After several charge/discharge cycles, the anode material cracks, leading to failure of the entire battery. Thus, crystalline silicon is unsuitable for designing lithium-ion current sources. It would seem that the situation can be corrected by relying on a strong carbon-silicon bond, i.e., by introducing carbon atoms into the silicon material. In particular, carbon can be used as a sealing layer covering the surface of a silicon electrode [3]. This design effectively compensates the change in volume and largely contributes to the preservation of capacity [4]. However, such a material is not sufficiently resistant to dynamic cycles that accompany the operation of an electrochemical device. In addition, the strong tendency to bind Si and C creates a tendency to form silicon carbide (SiC) [5]. The studies carried out have shown that by using a SiC anode it is possible to achieve a sufficiently high reversible capacity (e.g., 1200 mA h g^{-1} for 200 cycles) [6]. However, the problem of increasing the life cycle time of such an electrode still remains unresolved.

Silicene can withstand large armchair, zigzag, and biaxial deformations (>0.15) [7]. The second-order elastic constants and in-plane Young's modulus also indicate that silicene is mechanically stable. The mechanical properties of silicene exhibit isotropic behavior. Young's modulus of silicene in both the zigzag and armchair directions is close to 199.3 GPa, and Poisson's ratio is 0.17 [8]. At the same time, crystalline silicon is not an elastically isotropic material [9]. The values of Young's modulus and Poisson's ratio for it are 140–180 GPa and 0.265–0.275, respectively. Silicene inherits the electrochemical properties of silicon. However, the capacity of the silicene electrode may be limited by its strength.

Molecular dynamics experiments have shown that silicene (when placed on various metal substrates (Ag, Ni, Cu) and on graphene) can remain stable during lithiation/delithiation cycles [10–14]. Silicene is not destroyed and returns to its original volume. In this case, defect-free silicene can have higher stresses and lower capacitance than silicene modified with vacancy defects [15]. Silicene doped with phosphorus (through transmutation) exhibits extraordinary stability and improved charge characteristics during lithiation when it is on a nickel substrate doped with copper [16, 17] or on a graphite substrate doped with nitrogen [18]. Note that stable metal (Au, Cu, Ni, Pd) coatings can also be obtained on a graphite substrate, which retain their integrity during hydrogen adsorption [19, 20].

There are still few studies on the mechanism of the electrochemical reaction of the SiC anode with Li^+ [6, 21].

There is an opinion that during the interaction of SiC with Li^+ a conversion reaction takes place, i.e., first SiC is decomposed into elemental Si. This is a reversible reaction. The Li^+ ion can reversibly react with Si [21]. Most often, SiC is used for LIB anodes in the form of nanosized particles and wire [22, 23], while in microelectronics, the SiC film is most often used. Note that the use of a SiC film as an anode material has a number of advantages, including higher uniformity and rate of lithium deposition. However, the use of a SiC film as an LIB anode requires further study.

In this paper, we study the applicability of the hybrid material obtained by combining a thin SiC film with two-layer silicene as an anode material for an LIB. Porous silicene whose pores are bi-, tri-, and hexavacancies is used for this purpose. In this case, the intercalation of the system with lithium is carried out in a vertical way; i.e., the lithium ions, which primarily fill the two-layer defective silicene, are directed perpendicularly to its surface. This method of filling a silicene anode with lithium is more gentle and almost unexplored [24].

The aim of this paper is to study the intercalation of lithium ions into a hybrid anode made in the form of a defective two-layer silicene on a two-dimensional SiC substrate. The main attention in this study is paid to the study of structural changes occurring in the 4H-SiC film after vertical intercalation.

COMPUTER MODEL

To date, more than 250 SiC polymorphs have been identified [25]. The structural, elastic, and electronic properties of 2H-SiC and 4H-SiC polytopes have been studied most carefully. It is these polytopes that have the most favorable structural, elastic, and electronic behavior. The structure of 2H-SiC has a direct analogy with the wurtzite structure. It consists only of elements A and B, stacked in the form ABABAB. In the 4H-SiC structure, the stacking period for elements A and B, the second half of which differs from the stacking of 2H-SiC, is twice as long. This difference is expressed in the twisting of the elements, so that an ABCB stack is formed in the 4H-SiC modification [25]. The total energy of this modification is slightly lower than the corresponding 2H-SiC modification; i.e., the 4H-SiC structure is more stable.

The model of the combined silicene/SiC anode was constructed as follows. The SiC substrate was represented by a thin film of the 4H modification of hexagonal SiC with lattice constants $a = 0.3073$ nm and $c = 1.0053$ nm, and it contained 6000 atoms. Hexagonal rings C covered the upper surface of the substrate on which the two-layer silicene was placed. A perfect silicene sheet contained 528 Si atoms. However, the simulation was carried out using defective silicene. In each sheet of silicene, nine vacancy defects were distributed approximately evenly over its surface. The silicene sheet could be filled with bi-, tri-, or hexavacancies. Therefore, depending on the type of defects placed on the sheet, it was formed by 510, 501, or 474 atoms. Silicene had a flower structure, which was experimentally observed on an Ag(111) substrate [26]. In other words, the unit cell of silicene contained 18 atoms, six of which rose above the rest, moving away from them by 0.74 Å. The silicene sheets were stacked with an offset, reproducing Bernal's ABAB stacking ... In this case, the protruding six atoms of the unit cells of the silicene sheets were turned outward. The gap between the silicene sheets was 0.75 nm. It was shown in [27–29] that such a gap is optimal for horizontal lithium intercalation. It was at this gap that the maximum filling of the channel with lithium was observed, since, on the one hand, it was possible to move the Li^+ ions along the channel, and on the other hand, a high adhesion of the ion to the channel walls was achieved, which prevented the release of Li^+ from the channel. The gap between the lower silicene sheet and the substrate was 0.27 nm; i.e., it had the same significance as in modeling the two-layer silicene on a graphite substrate system [30, 31].

The interactions between Si atoms inside the silicene sheets and Si and C atoms in the SiC compound were described using the proven Tersoff potential [32], which has proven itself well for modeling two-dimensional systems [10–13]. The interaction between Si atoms belonging to different silicene sheets, as well as between Si atoms of silicene and substrate atoms (C and Si), was described by the Morse potential with parameters from [33]. The Lennard–Jones potential was applied to describe the Li–Li, Li–Si, Li–C interactions with the parameters from [34].

All particles in the system, with the exception of Si atoms located along the perimeter of the silicene sheets, moved in accordance with the law of Newtonian mechanics. The Si atoms that formed the perimeter of the silicene sheets were fixed to maintain the overall stability of a very small system (from 7094 to 7171 atoms) and the permeability of the silicene channel. The equations of motion were integrated with the time step $\Delta t = 10^{-16}$ s. In contrast to the works [27–29], this study presents the results of vertical filling a silicene channel with lithium. This method turned out to be preferable to horizontal filling, as it resulted in a smaller distortion of the silicene channel. Initially, the Li^+ ions were randomly placed above the top sheet of silicene at a height of 0.6 nm. They were sequentially sent towards the simulated anode at regular intervals of 10 ps. During this time, the ion fell into the sphere of action of the Si atoms. Before reaching the top sheet of silicene, the Li^+ ion moved vertically downwards under the action of a constant electric field with a strength of 10^4 V/m. Once on the surface of the top sheet of silicene, the ion moved along it until it found a pore through which it could pass further down. Then, under the action of the field, the ion could

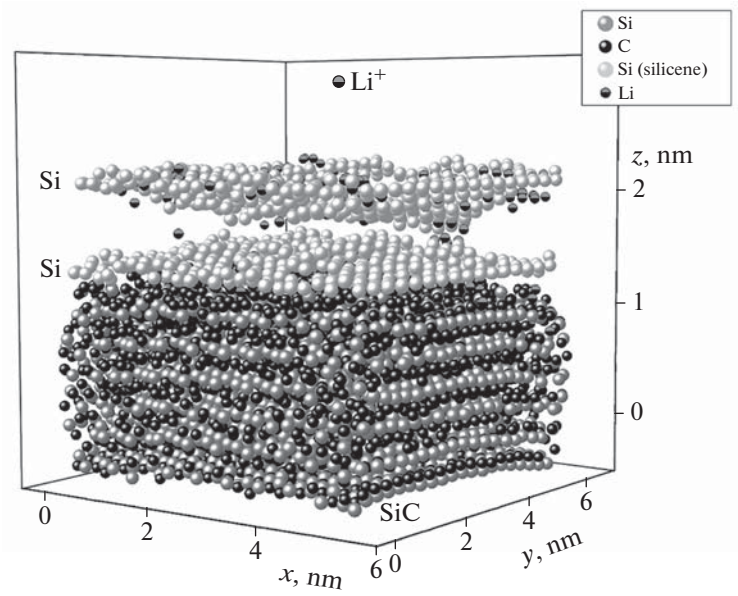

Fig. 1. Silicene/SiC system after it is vertically filled with lithium in 1.5 ns; each sheet of two-layer silicene contains nine divacancies.

move along the surface of the bottom sheet until it met the pore located in this sheet, and even fall under the bottom sheet, passing through this pore. Some of the Li^+ ions (Li atoms) are retained in the silicene channel or fixed on any of the silicene sheets. The Li^+ ion lifetime was determined by an interval of 10 ps, after which it turned into a neutral atom and lost the ability to "feel" the electric field. According to the terahertz radiation theory, the Li^+ ion should turn into a neutral atom in a medium with a negative electric potential in just 1 ps [35]. The total intercalation time was 1.51 ns. During this time, 151 Li^+ ions were launched towards the silicene/SiC system.

The self-diffusion coefficient was calculated from the root-mean-square displacement of atoms $\left\langle [\Delta \mathbf{r}(t)]^2 \right\rangle$:

$$D = \lim_{t\to\infty} \frac{1}{2\Gamma t} \left\langle [\Delta \mathbf{r}(t)]^2 \right\rangle,$$

where $\Gamma = 3$ is the space dimension and the angle brackets denote time averaging.

In a computer experiment, information about the detailed structure of small objects can be obtained based on the construction of Voronoi polyhedra (VP). In this case, the short-range order in the arrangement of atoms is represented in the form of statistical distributions of the VP over the number of faces and faces over the number of sides, or in the form of the distribution of angles formed by pairs of geometric neighbors with the central atom (the center of the VP). These distributions together give an idea of the spatial (three-dimensional) structure of atomic packings, which cannot be obtained using the one-dimensional radial distribution function.

All the calculations were performed by the molecular dynamics method using parallel computing and the LAMMPS open access code [36]. The calculations were carried out on a hybrid computer cluster of the URAN type at Krasovskii Institute of Mathematics and Mechanics, Ural Branch, Russian Academy of Sciences with a peak performance of 216 Tflop/s and 1864 CPU.

CALCULATION RESULTS

The configuration of the silicene/SiC system after intercalation of 151 Li^+ ions is shown in Fig. 1. It can be seen that the silicene sheets were significantly deformed during intercalation. A bulge appeared on each of them, directed inside the channel formed by these sheets. The curvature of the sheets hinders the movement of Li atoms along the channel. The lower sheet of silicene adjacent to the substrate is deformed to a lesser extent than the upper one. The thermal motion of the Si and C atoms led to the distortion of the atomic rows in the SiC film (substrate). No signs of destruction of the silicene/SiC system were observed.

The horizontal projections of silicene sheets constructed after the intercalation of 151 lithium ions indicate the preservation of defects with satisfactory preservation of their shape after the intercalation. Figure 2 shows silicene sheets with trivacancies together with Li atoms attached to them after intercalation is complete. As can be seen from this figure, in general, the silicene sheets retained their integrity and atomic

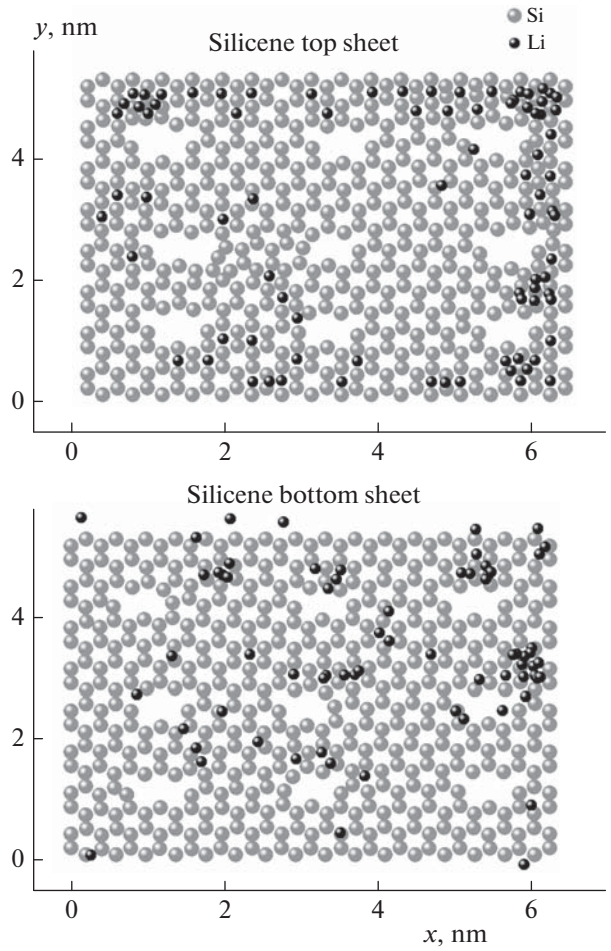

Fig. 2. Horizontal projections of the top and bottom sheets of silicene with trivacancies after vertical intercalation of Li^+ ions in 1.51 ns; lithium atoms that did not pass into the silicene channel (top) and got into it (bottom) are shown by black circles.

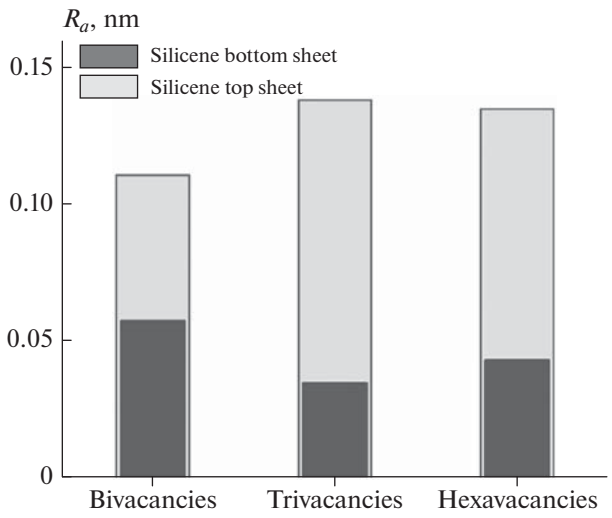

Fig. 3. Roughness of silicene sheets containing various vacancy defects in the silicene/SiC system after it is filled with lithium in 1.51 ns.

structure. The formation of islands of lithium atoms, which are mainly located on the periphery of the outer surface of the upper and lower sheets, is observed. In the latter case, they are preserved inside the silicene channel. In the middle part of the sheets, the Li atoms are mostly dispersed.

Figure 3 shows that the roughness of the top and bottom sheets of silicene is not the same. The silicene sheet in direct contact with the substrate is less rough by a factor of 2 to 4 times than the overlying sheet. Moreover, the minimum value of the roughness parameter R_a of the lower sheet is achieved in the presence of trivacancies in it, and the maximum is achieved when the defects are bivacancies. For the top sheet, in contrast, the presence of trivacancies in it creates the maximum roughness, while the top sheet with bivacancies is characterized by the minimum roughness. Such behavior of R_a is caused by the stabilizing effect of the substrate on the bottom sheet of silicene and the impact of intercalated lithium ions on the top sheet.

The partial radial distribution functions $g_{\mathrm{Si-Li}}(r)$ reflect on average the nature of the arrangement of Li atoms around the Si atoms. The higher the first peak of this function at close values of its half-width the more significantly the first coordination sphere of Si atoms is filled with Li atoms. Figure 4 shows that the intensity of the first peak of the function $g_{\mathrm{Si-Li}}(r)$ decreases as the type of defects in silicene changes from bivacancies to hexavacancies, i.e., with an increase in their size. This means that the filling density of the first Si coordination sphere with Li atoms decreases with an increase in the size of defects in the walls of the silicene channel. The height of the first peak of the function $g_{\mathrm{Si-Li}}(r)$ did not increase, and the obtained dependence on the type of defects was preserved when the equivalent filling of the identical silicene/SiC system with lithium was performed in the horizontal direction. The function $g_{\mathrm{Si-Li}}(r)$, obtained by horizontal intercalation in the presence of hexavacancies in silicene is shown in Fig. 4 as an example. Thus, the filling density of the first coordination sphere for Si atoms with lithium is mainly determined by the type of defects created in the silicene sheets.

The angular distributions of the nearest geometric neighbors in the Si- and C-subsystems of the SiC substrate indicate a significant difference in the short-range order of the atoms of these subsystems (Fig. 5). This difference manifests itself for all types of vacancy defects present in silicene. In the case of the Si subsystem, clearly pronounced peaks of the φ distribution are observed at angles of 38°, 51°, 63°, and 94°. There are also several weakly pronounced peaks correspond-

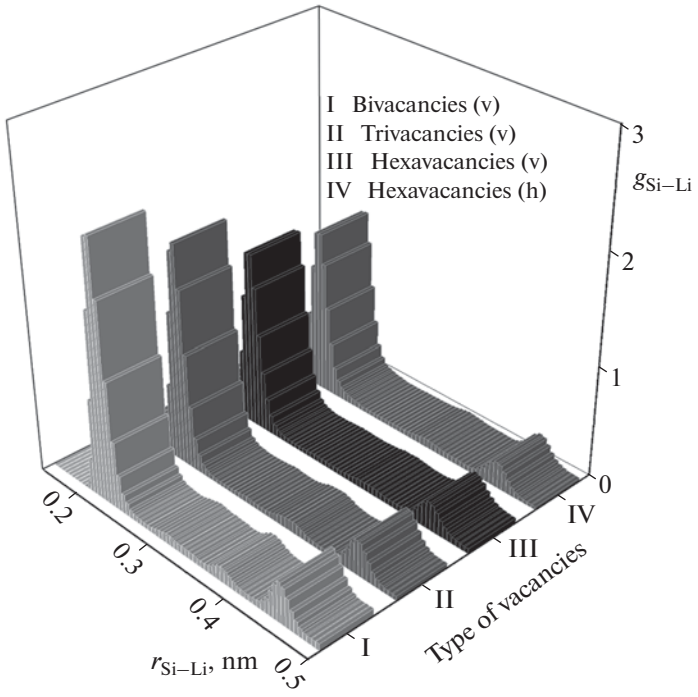

Fig. 4. Partial radial distribution functions $g_{Si-Li}(r)$, obtained after (c) vertical and (d) horizontal intercalation of lithium for silicene/SiC systems in the walls of silicene channels with vacancy defects.

ing to larger angles (111°, 123°, and 152°). This type of angular distribution indicates the presence of a certain regularity in the packing of the Si atoms. At the same time, for the C subsystem, the angular distributions, regardless of the type of defects present in silicene, have a much smoother shape. Only two weakly protruding peaks at 63° and 94° are present in these φ distributions. Two more poorly visible protrusions are found at angles of 123° and 153°. These distributions indicate the presence of a very small fraction of regularity in the packing of atoms of the C subsystem. Basically, the packing of C atoms in the substrate appears irregular. The resulting angular distributions are of the same type for different types of vacancies in silicene; thus, the φ-distributions obtained in the presence of trivacancies in Fig. 5 are not shown.

The distribution of the VP over the number of faces (*n*-distribution), which shows the quantitative composition of the geometric neighbors, is an important topological characteristic (Fig. 6). The *n*-distributions obtained by vertically filling the system with lithium indicate that, in the case of the Si subsystem, the Si atoms are most often surrounded by 11 similar neighbors, while for the C subsystem, the maximum neighborhood between the same type of C atoms is determined by the number 12. Furthermore, the *n*-distributions for the C-subsystem extend up to $n = 18$, while the extent of such distributions for the Si subsystem is limited by the number $n = 15$. In other words, *n*-the spectrum for the Si subsystem is poorer than for the C subsystem. The calculated mathematical expectations and asymmetries for *n*-spectra of the Si- and C-subsystems differ significantly (Table 1). At the same time, the difference in the standard deviations of the *n*-distributions of such systems is not as significant. Note that the asymmetry for the *n*-distributions of the C-subsystem has the opposite (negative) sign with respect to this characteristic for the corresponding distributions of the Si-subsystem.

The VP faces distributions over the number of sides (*m*-distributions) have an even weaker dependence on the type of vacancy defects present in silicene compared to the *n*-distributions (Fig. 7). The mathematical expectations, standard deviations, and asymmetry of the distributions of VP faces by the number of sides

Table 1. Expected value (μ), standard deviation (σ), and asymmetry (A) of the distributions of the VP by the number of faces and faces by the number of sides

Subsystem characteristics	$\mu(n)$	$\sigma(n)$	$A(n)$	$\mu(m)$	$\sigma(m)$	$A(m)$
Si (bivacancies)	9.28	3.966	0.490	4.88	2.474	0.976
Si (trivacancies)	9.23	4.385	0.757	4.90	2.463	0.968
Si (hexavacancies)	9.30	3.962	0.478	4.89	2.991	1.099
C (bivacancies)	11.23	4.478	–0.140	5.14	2.848	1.035
C (trivacancies)	11.18	4.476	–0.112	5.14	2.850	1.037
C (hexavacancy)	11.16	4.475	–0.098	5.14	2.850	1.037

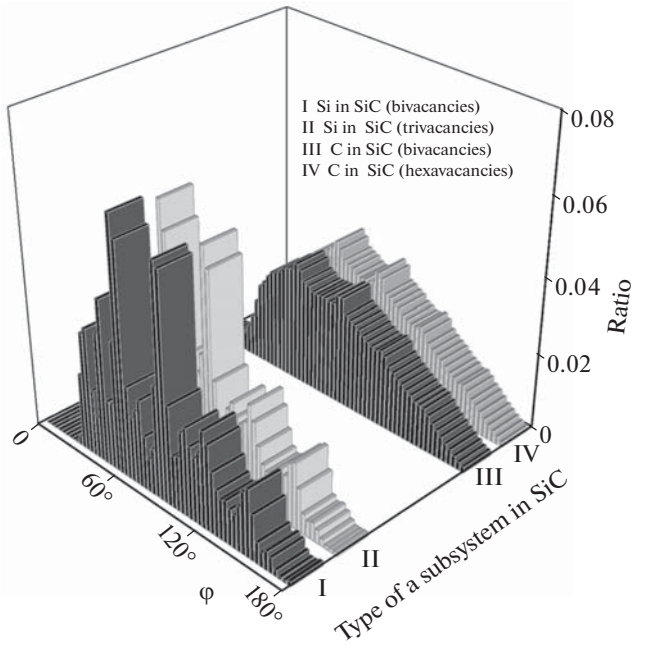

Fig. 5. Angular distribution of the nearest geometric neighbors for the Si- and C-subsystems of SiC, which acts as a substrate for a defective two-layer silicene vertically intercalated with lithium for 1.51 ns.

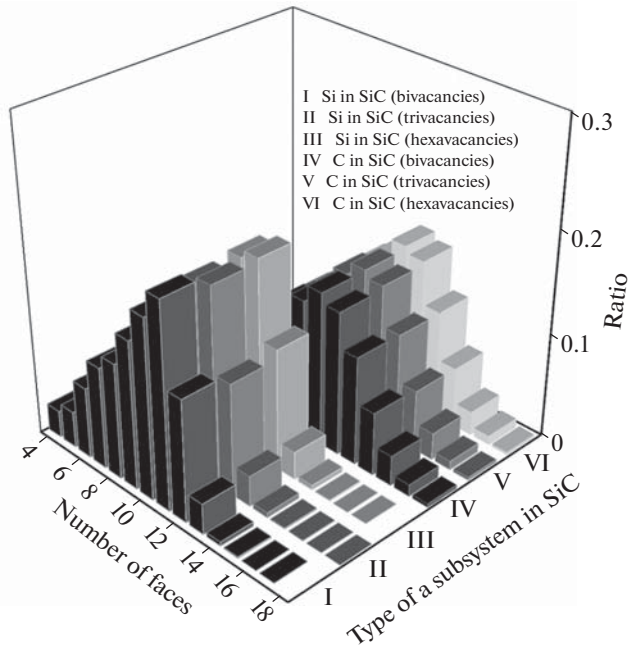

Fig. 6. The distribution of VP over the number of faces, constructed for the Si- and C-subsystems of SiC, after the silicene/SiC system is vertically filled with lithium in 1.51 ns; the types of defects in silicene are indicated in parentheses.

are presented in Table 1. As can be seen from this table, belonging to the C-subsystem is clearly shown by the set of parameters $\mu(m)$, $\sigma(m)$, and $A(m)$. However, in the case of the Si subsystem, when hexavacancies are in silicene, the values of the parameters $\sigma(m)$ and $A(m)$ deviate from the characteristic values inherent in this group in the presence of bi- and trivacancies in silicene. Note that in all cases the maximum m-distributions fall on the value $m = 5$. The dominance of the rotational symmetry of the 5th order is typical for the irregular packing of atoms. However, in this case, the appearance of a maximum in the m-distributions at $m = 5$ is related to the high level of small-scale thermal fluctuations in the considered subsystems.

After excluding the small edges in the VP with length $l < 0.5\,\overline{l}$, where $\overline{l}$ is the average length of the edge of the VP, the distribution of faces according to the number of sides takes the form shown in Fig. 8. As can be seen from this figure, the number of four-sided faces becomes predominant in the case of the Si subsystem. However, for the C subsystem, the faces with $m = 5$ still prevail. Thus, the disordering factor manifests itself to a greater extent in the C subsystem than in the Si subsystem.

DISCUSSION

The results presented in this study show that the vertical intercalation of lithium did not lead to significant destruction of the silicene sheets, although they were somewhat deformed. The direction (vertical or horizontal) of the intercalation performed had no effect on the degree to which lithium filled the anode;

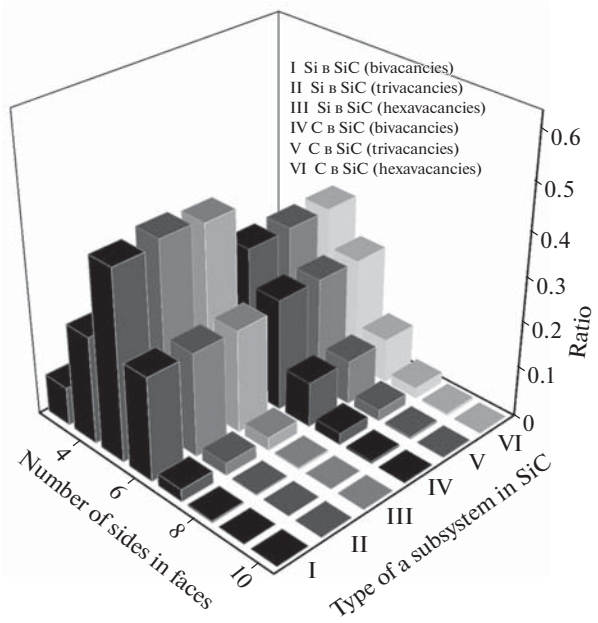

Fig. 7. Face distribution of VP according to the number of sides constructed for Si- and C-subsystems of SiC after the silicene/SiC system is vertically filled with lithium in 1.51 ns; the types of defects in silicene are indicated in parentheses.

Table 2. Average values of the lithium self-diffusion coefficient for vertical intercalation

Type of vacancies in Silicene	D_{Li}, 10^{-5} cm^2/s
Bivacancies	3.16
Trivacancies	2.88
Hexavacancies	3.05

in both directions, the occupancy was almost the same. However, with horizontal filling, a small part of lithium entered the SiC substrate, and the profile of the silicene channel was distorted more strongly than with vertical intercalation.

The process of vertical lithiation is accompanied by the appearance of stresses in the material in which lithium ions are intercalated. In the model studied here, the upper part of the anode is subjected to the strongest action of lithium, i.e., two-layer silicene. The stresses in silicene in the process of incorporating lithium arise due to the inhomogeneity of the structure related to the presence of vacancy defects, as well as the inhomogeneous compression and tension of silicene related to its interaction with lithium, which manifests itself in the appearance of an even stronger stress when the silicene channel is filled with lithium with perfect walls [37]. Lithium can create both elastic and inelastic stresses in silicene. It was experimentally shown that the stress created inside the Li_xSi compound turned out to be much lower than the yield stress [38]. A similar conclusion was obtained by simulating the molecular dynamics of filling a silicene channel with lithium on metal [39] and graphite [40] substrates.

There are two points of view on the mechanism of diffusion of guest atoms in a stressed material. These mechanisms can be described based on the free energy diagram. In the first case, diffusion is caused by the stress induced by a shift in the activation energy barrier [41, 42]. In this case, the reaction rate depends on the difference between the free energies of the ground and transition states, i.e., on the activation energy. In the second case, diffusion is explained by the change in the difference between the free energies of the substrate and the material (i.e., silicene) under the action of the applied stress [43, 44]. In other words, the difference in free energy is the driving force behind the reaction. When considering the diffusion of lithium in energized silicene, both of these effects must be taken into account. The diffusion coefficient of Li in silicene (D_{Li}) is the key parameter that determines the lithiation time. In turn, the Li concentration gradient affects the intercalation stress. The lithium self-diffusion coefficient is a strongly fluctuating function of the number of intercalated Li atoms. The average values of this characteristic, obtained over the entire time interval of intercalation (1.51 ns), are presented in Table 2. As can be seen from this table, the lowest self-diffusion coefficient is observed in the presence of trivacancies in silicene.

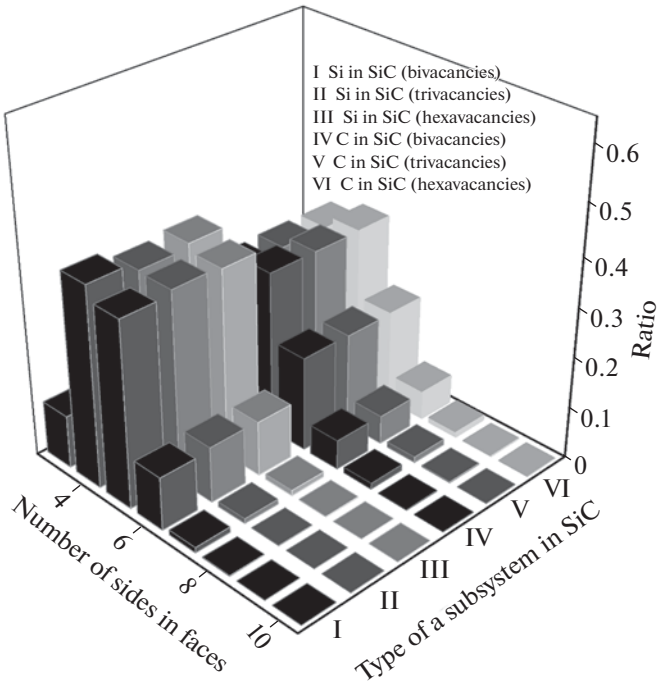

Fig. 8. The distribution of faces of rough VP by the number of sides constructed for the Si and C subsystems of SiC after the silicene/SiC system is vertically filled with lithium in 1.51 ns; the types of defects in silicene are indicated in parentheses.

The slowing down of lithium diffusion in silicene is due to the fractal shape of these defects, which leads to a significant local deformation of silicene upon the incorporation of lithium. In contrast, in the case of smaller defects, i.e., bivacancies, the local deformation of silicene is minimal, and the self-diffusion coefficient reaches the highest value. Although hexavacancies are the largest of the considered defects, their shape is not as zigzagged as that of trivacancies. The Li^+ ions passing through hexavacancies affect silicene to a lesser extent than ions passing through tri- or bivacancies. However, the silicene with hexavacancies is weaker than the silicene with bivacancies due to the removal of a larger number of Si atoms during the formation of defects and the retention of a smaller number of covalent bonds. Therefore, during the intercalation of lithium, silicene with bivacancies experiences smaller local deformations than silicene with hexavacancies. Note that the self-diffusion coefficient of lithium atoms moving along a separate sheet of silicene is 5.0×10^{-5} cm^2/s [45], and performing horizontal intercalation under the same conditions as in the present study leads to an increase in the D_{Li} value on average of 38%.

Our calculations indicate the possibility of a structural transition occurring in an SiC film subjected to an external action. Such a transition can be initiated by a more mobile C subsystem in which the crystal order in the atomic packing is less stable than in the Si subsystem. It is possible that the polycrystalline microstructure will correspond to a more stable state of the SiC film exposed to lithium-filled two-layer silicene. An experimental study of the crystallization observed upon the annealing of thin amorphous SiC films made it possible to establish the mechanism of the process, which occurs through the nucleation and growth of crystalline grains with an activation energy of 5.1 eV [46]. The crystallized films had a polycrystalline structure.

CONCLUSIONS

The vertical intercalation of lithium into a combined silicene/SiC anode was studied by the method of molecular dynamics. It is shown that the filling density of the first Si coordination sphere is higher the smaller the pore size in the silicene sheets. First of all, lithium atoms deposited on silicene fill the peripheral part of the upper sheet, being located along its perimeter. However, for the lower sheet, its middle part is first filled with lithium. During intercalation, the top sheet of silicene experiences significantly greater vertical deformations than the bottom sheet. This is manifested in the high degree of roughness of the top sheet. After intercalation, the roughness of the bottom sheet of silicene decreases; it becomes less rough than it was originally. The silicon subsystem of the SiC substrate is less disordered than the C subsystem. This is confirmed by the shape of the angular distributions, as well as by the distributions of VP in terms of the number of faces and faces in terms of the number of sides. The exclusion of small edges in the VP leads to a situation where the 4th order rotational symmetry prevails for the Si subsystem, while the 5th order rotational symmetry is preserved for the C subsystem. The diffusion of lithium atoms in the system proceeds most intensively when bivacancies are present in silicene sheets, and the weakest diffusion is observed when trivacancies are present in silicene. Vertical filling with lithium can be used for a combined silicene/SiC anode when charging a lithium-ion battery.

FUNDING

This study was carried out on the topic of state task no. 122020100205-5 (FUME-2022-0005) and under agreement no. 075-03-2022-011 of 14 January, 2022 (FEUZ-2020-0037).

REFERENCES

1. A. Y. Galashev and K. A. Ivanichkina, Phys. Chem. Chem. Phys. **21** (23), 12310 (2019). https://doi.org/10.1039/C9CP01571J
2. A. Galashev, K. Ivanichkina, K. Katin, and M. Maslov, Computation **7**, 60 (2019). https://doi.org/10.3390/computation7040060Y
3. Y. Yang, J. G. Ren, X. Wang, et al., Nanoscale **5** (18), 8689 (2013). https://doi.org/10.1039/C3NR02788K
4. C. Qi, S. Li, Z. Yang, et al., Carbon **186**, 530 (2022). https://doi.org/10.1016/j.carbon.2021.10.062
5. X. H. Chang, W. Li, J. F. Yang, et al., J. Mater. Chem. A **3** (7), 3522 (2015). https://doi.org/10.1039/C4TA06334A
6. T. S. Kumari, D. Jeyakumar, and T. P. Kumar, RSC Adv. **3** (35), 15028 (2013). https://doi.org/10.1039/C3RA40798E
7. Q. Peng, X. -D. Wen, and S. De, RSC Adv. **3**, 13772 (2013). https://doi.org/10.1039/C3RA41347K
8. S. H. Yoo, B. Lee, and K. Kang, Nanotecnology **32** (29), 295702 (2021). https://doi.org/10.1088/1361-6528/abf26d
9. J. J. Wortman and R. A. Evans, J. Appl. Phys. **36**, 153 (1965). https://doi.org/10.1063/1.1713863
10. A. E. Galashev, O. R. Rakhmanova, K. A. Ivanichkina, and Y. P. Zaikov, Lett. Mater. **8** (4), 463 (2018). https://doi.org/10.22226/2410-3535-2018-4-463-467
11. A. Y. Galashev, K. A. Ivanichkina, and O. R. Rakhmanova, Comput. Mater. Sci. **200**, 110771 (2021). https://doi.org/10.1016/j.commatsci.2021.110771
12. A. Y. Galashev, Solid State Ionics **357**, 115463 (2020). https://doi.org/10.1016/j.ssi.2020.115463
13. A. E. Galashev, O. R. Rakhmanova, and A. V. Isakov, Khim. Fiz. **39** (7), 72 (2020). https://doi.org/10.1134/S1990793120060044

14. A. E. Galashev, O. R. Rakhmanova, and Yu. P. Zaikov, Fiz. Tverd. Tela **58** (9), 1786 (2016). http://elibrary.ru/item.asp?id=27368752.
15. A. E. Galashev and O. R. Rakhmanova, Teplofiz. Vys. Temp. **54** (1), 13 (2016). https://doi.org/10.7868/S0040364415050129
16. A. Y. Galashev, K. A. Ivanichkina, A. S. Vorob'ev, et al., Int. J. Hydrogen Energy **46** (32), 17019 (2021). https://doi.org/10.1016/j.ijhydene.2020.11.225
17. A. Y. Galashev, Int. J. Comput. Methods **18** (9), 2150032 (2021). https://doi.org/10.1142/S0219876221500328
18. A. E. Galashev, O. R. Rakhmanova, K. P. Katin, M. M. Maslov, and Yu. P. Zaikov, Khim. Fiz. **39** (11), 80 (2020). https://doi.org/10.31857/S0207401X20110047
19. M. V. Grishin, A. K. Gatin, S. Yu. Sarvadii, et al., Khim. Fiz. **39** (7), 63 (2020). https://doi.org/10.31857/S0207401X20070067
20. N. V. Dokhlikova, A. K. Gatin, S. Yu. Sarvadii, et al., Khim. Fiz. **40** (7), 67 (2021). https://doi.org/10.31857/S0207401X21070025
21. H. T. Zhang and H. Xu, Solid State Ionics **263**, 23 (2014). https://doi.org/10.1016/j.ssi.2014.04.020
22. Y. W. Hu, X. S. Liu, X. P. Zhang, et al., Electrochim. Acta **190**, 33 (2016). https://doi.org/10.1016/j.electacta.2015.12.211
23. M. Shiratani, K. Kamataki, G. Uchida, et al., Mater. Res. Soc. Symp. Proc. **1678**, 7 (2014). https://doi.org/10.1557/opl.2014.742
24. M. Rajapakse, B. Karki, U. O. Abu, et al., NPJ 2D Mater. Appl. **5**, 30 (2021). https://doi.org/10.1038/s41699-021-00211-6
25. Md. Nuruzzaman, M. Ariful Islam, M. Alam Ashraful, M. A. Hadi Shah, and A. M. M. Tanveer Karim, Int. J. Eng. Res. Appl. **5** (5), 48 (2015). ISSN: 2248-9622.
26. K. Kawahara, T. Shirasawa, R. Arafune, et al., Surf. Sci. **623**, 25 (2014). https://doi.org/10.1016/j.susc.2013.12.013
27. A. E. Galashev and K. A. Ivanichkina, Russ. J. Phys. Chem. A **93** (4), 765 (2019). https://doi.org/10.1134/S0044453719040137
28. A. Y. Galashev and K. A. Ivanichkina, ChemElectroChem **6** (5), 1525 (2019). https://doi.org/10.1002/celc.201900119
29. A. Y. Galashev and K. A. Ivanichkina, J. Electrochem. Soc. **165** (9), A1788 (2018). https://doi.org/10.1149/2.0751809jes
30. A. E. Galashev, O. R. Rakhmanova, and K. A. Ivanichkina, J. Struct. Chem. **59** (4), 877 (2018). https://doi.org/10.1134/S0022476618040194
31. A. Y. Galashev, K. A. Ivanichkina, K. P. Katin, and M. M. Maslov, ACS Omega **5** (22), 13207 (2020). https://doi.org/10.1021/acsomega.0c01240
32. J. Tersoff, Phys. Rev. B **38** (14), 9902 (1988). https://doi.org/10.1103/PhysRevB.38.9902
33. T.-E. Fang and J.-H. Wu, Comput. Mater. Sci. **43** (4), 785 (2008). https://doi.org/10.1016/j.commatsci.2008.01.066
34. M. K. Song, S. D. Hong, and T. N. Kyoung, J. Electrochem. Soc. **148** (10), A1159 (2001). https://doi.org/10.1149/1.1402118
35. Y. Pan and Y. A. Gover, J. Phys. Commun. **2** (11), 115026 (2018). https://doi.org/10.1088/2399-6528/aae2ec
36. S. Plimpton, J. Comput. Phys. **117** (1), 1 (1995). https://doi.org/10.1006/jcph.1995.1039
37. A. E. Galashev and K. A. Ivanichkina, Phys. Solid State **61** (2), 233 (2019). https://doi.org/10.1134/S1063783419020136
38. K. Zhao, G. A. Tritsaris, M. Pharr, et al., Nano Lett. **12** (8), 4397 (2012). https://doi.org/10.1021/nl302261w
39. A. Kushima, J. Y. Huang, and J. Li, ACS Nano **6** (11), 9425 (2012). https://doi.org/10.1021/nn3037623
40. V. I. Levitas and H. Attariani, Sci. Rep. **3**, 1615 (2013). https://doi.org/10.1038/srep01615
41. V. Sukharev, E. Zschech, and W. D. Nix, J. Appl. Phys. **102** (5), 053505 (2007). https://doi.org/10.1063/1.2775538
42. Y. F. Gao, M. Cho, and M. Zhou, J. Mech. Sci. Technol. **27**, 1205 (2013). https://doi.org/10.1007/s12206-013-0401-7
43. G. Bucci, S. P. V. Nadimpalli, V. A. Sethuraman, A. F. Bower, and P. R. Guduru, J. Mech. Phys. Sol. **62**, 276 (2014). https://doi.org/10.1016/j.jmps.2013.10.005
44. J. Chakraborty, C. P. Please, A. Goriely, and S. J. Chapman, Int. J. Solid Struct. **54**, 66 (2015). https://doi.org/10.1016/j.ijsolstr.2014.11.006
45. B. Mortazavia, A. Dianatb, G. Cunibertib, and T. Rabczuka, Electrochim. Acta **213**, 865 (2016). https://doi.org/10.1016/j.electacta.2016.08.027
46. L. Calcagno, P. Musumeci, F. Roccaforte, C. Bongiorno, and G. Foti, Appl. Surf. Sci. **184** (1–4), 123 (2001). https://doi.org/10.1016/S0169-4332(01)00487-1